Title: Respiratory Airway Secretory Cells act as Immune Sentinels in Human Distal Airways

Authors: Jiaqi Sun[1]†, Shisheng Jiang[1]†, Hui Sun[1], Xiaoxiao Xie[1], Hao Meng[1], Dong Wang[4], Hongjie Yao[1], Hui Zheng[5], Weijie Guan[1,3], Jincun Zhao[1,3]*, Wei Kevin Zhang[1]*, Tao Xu[1]*, Huisheng Liu[1,2]*

Affiliations:

[1]School of Biomedical Engineering, School of Pharmaceutical Sciences, Guangzhou National Laboratory, Guangzhou Medical University; Guangzhou, China.

[2]Department of Endocrinology and Metabolism, Xinjiang Clinical Research Center for Diabetes, Xinjiang Endocrinology Diabetes Institute, Xinjiang Key Laboratory of Cardiovascular Homeostasis and Regeneration Research, People's Hospital of Xinjiang Uygur Autonomous Region; Urumqi, China.

[3]State Key Laboratory of Respiratory Disease, National Clinical Research Center for Respiratory Disease, Guangzhou Institute of Respiratory Health, The First Affiliated Hospital of Guangzhou Medical University; Guangzhou, China.

[4]GMU-GIBH Joint School of Life Sciences, Guangzhou Medical University; Guangzhou, China.

[5]Center for Cell Lineage Technology and Bioengineering, Guangdong Provincial Key Laboratory of Stem Cell and Regenerative Medicine, Guangdong-Hong Kong Joint Laboratory for Stem Cell and Regenerative Medicine, GIBH-CUHK Joint Research Laboratory on Stem Cell and Regenerative Medicine, GIBH-HKU Guangdong-Hong Kong Stem Cell and Regenerative Medicine Research Centre, China-New Zealand Belt and Road Joint Laboratory on Biomedicine and Health, Guangzhou Institutes of Biomedicine and Health, Chinese Academy of Sciences; Guangzhou, China

*Corresponding author. Email: liu_huisheng@gzlab.ac.cn; xu_tao@gzlab.ac.cn; zhaojincun@gird.cn; zhang_wei@gzlab.ac.cn

†These authors contributed equally to this work.

Abstract: Pulmonary immunity in the human distal respiratory airways is essential for lung function but remains less explored. Here we report that respiratory airway secretory (RAS) cells, a newly identified lung epithelial population unique to humans and large mammals, act as immune sentinels in the distal airways by safeguarding against infection and injury. Leveraging human pluripotent stem cell-derived lung organoids, animal models, and clinical specimens, we elucidate that RAS cells arise from distal lung progenitors and exhibit context-dependent immune competence. Upon viral or bacterial challenge, RAS cells display interferon-mediated or TLR5-dependent defense responses, respectively. In chronic obstructive pulmonary disease, they produce elevated adaptive immune responses. Notably, complement C3 is upregulated under these conditions and is suppressed by a selective TLR5 inhibitor. Our findings reveal RAS cells as previously unrecognized sensors and effectors of mucosal immunity at human distal airways, highlighting the TLR5–complement axis as a potential therapeutic target in lung disease.

Main Text: The human respiratory tract orchestrates air exchange while defending against pathogens through specialized epithelial cells (*1, 2*). Unlike mice, humans possess distinct distal airway structures, termed respiratory airways (RAs) or terminal and respiratory bronchioles (TRBs), that bridge the conducting airways to the alveolar sacs. These distal structures are essential for efficient respiration (*3, 4*) yet are frequent targets of injury in respiratory diseases. Chronic obstructive pulmonary disease (COPD) (*5-7*), pulmonary fibrosis (*8, 9*), and viral infections (*10, 11*) all provoke inflammation and remodeling of RAs, leading to impaired respiratory function and progressive deterioration. A limited understanding of immune regulation in RAs has hindered the development of effective therapies.

Recent studies have identified unique SCGB3A2-expressing secretory cells (SCs), termed RAS cells or TRB-SCs, in the human distal airways (*12*). These RAS cells serve as progenitors for alveolar type 2 (AT2) cells (*13*). Additional evidence suggests that AT2 cells differentiate into TRB-SCs via an intermediate AT0 state (*14*). However, due to the limited access to human distal airway tissue, the low abundance of these cells, and the lack of suitable models, their developmental origin and broader functional roles remain elusive.

Here we develop a human pluripotent stem cell (hPSC)-derived distal lung organoid system to generate and study RAS cells. These distal lung organoids recapitulate key developmental and structural features of the distal lung epithelium and serve as robust platforms for functional analysis. By combining single-cell transcriptomics, pathogen challenge assays, and analysis of clinical COPD specimens, we show that RAS cells arise from NKX2-1^{bright}SOX9^{bright} distal lung progenitors and acquire context-dependent immune competence. Specifically, RAS cells mount robust immune defense responses to respiratory pathogens. In COPD, RAS cells assume an immunologically active state. Notably, complement C3 emerges as a convergent effector across these conditions, which is the downstream of TLR5 signaling. Together, these findings establish RAS cells as previously unrecognized epithelial immune sentinels in the human distal airway and implicate the TLR5 – complement axis as a potential therapeutic target in chronic lung disease.

Robust Generation of Distal Lung Organoids

Human lung development relies on spatially distinct progenitor populations: SOX2^{bright}NKX2-1^{dim} proximal lung progenitor cells (p-LPC) drive airway differentiation, while SOX9^{bright}NKX2-1^{bright} distal lung progenitor cells (d-LPC) are critical for branching morphogenesis and alveologenesis (Fig. 1A) (*15-19*). To generate SOX9^{bright}NKX2-1^{bright} distal lung progenitors from hPSCs, we utilized and modified previously reported protocols for definitive endoderm (DE) and 3D anterior foregut endoderm (AFE) spheroid induction (fig. S1A) (*20*). Inspired by successful colon organoid systems that dissociate hindgut endoderm into Matrigel (*21*), we dissociated AFE spheroids into single cells and embedded them in 3D Matrigel droplets (Fig. 1B). This dissociation step dramatically increased organoid yield (>4-fold) and uniformity (fig. S1, B to E).

Transcript analysis of lung progenitor markers (*SOX2*, *SOX9*, *NKX2-1*) revealed that dissociation significantly upregulated *NKX2-1* expression (10- to 100-fold), with minimal changes in *SOX9* and *SOX2* levels (Fig. 1D, and fig. S1I). Triple immunostaining confirmed enrichment of SOX9^{bright}NKX2-1^{bright} cells in dissociation-treated cultures, whereas SOX2^{bright}NKX2-1^{dim} populations dominated untreated conditions (Fig. 1C). Flow cytometry further validated elevated NKX2-1 protein levels in dissociated organoids (fig. S1, F to H).

Aligning with embryonic lung gene expression patterns (*15*), we designated organoids from untreated conditions as proximal lung organoids (p-LOs) and those from dissociated cultures as distal lung organoids (d-LOs). The protocol consistently generated d-LOs across multiple hPSC lines, underscoring its robustness and broad applicability (fig. S1I).

Characterization of d-LOs

To validate the distal identity of d-LOs, we performed single-cell RNA sequencing (scRNA-seq) on 10,815 cells from p-LOs and d-LOs at day 8. Our analysis identified three cellular compartments: epithelial, mesenchymal, and neural cells (fig. S2, A and B). We then extracted and reclustered the epithelial cells for a more detailed investigation (Fig. 1, E and F, and fig. S2C). Six cell clusters were annotated based on their distinct molecular features: d-LPC, p-LPC, cycling, neuroendocrine, hindgut, and an unknown population. Notably, the d-LPC cluster was abundantly generated in d-LOs (43.01% in d-LOs and 0.71% in p-LOs; Fig. 1G), while p-LPC was enriched in p-LOs (12.33% in d-LOs and 37.29% in p-LOs; Fig. 1G), corroborating gene and protein expression data.

Benchmarking against human fetal lung datasets (*15*) further confirmed proximal-distal divergence (Fig. 1H and fig. S2F): p-LPC in p-LOs expressed proximal markers (e.g., *SOX2*, *DMD*, *SEMA3C*, *KREMEN1*, and *MIR99AHG*), while the d-LPC cluster in d-LOs upregulated distal regulators (e.g., *SOX9*, *ETV1*, *SOX6*, and *GATA*). Notably, ETV1 and SOX6 are human development-specific transcription factors involved in distal lung patterning (*15*). Gene Ontology analysis of differentially expressed genes (DEGs) within the p-LPC and d-LPC clusters reinforced their proximal and distal identities (fig. S2, D and E). Specifically, p-LPC genes are involved in cilium organization and assembly, while d-LPCs are enriched for genes associated with epithelial tube morphogenesis and branching morphogenesis, with high expression of *NKX2-1*, *SOX9*, *WNT7B* and low expression of *SFTPC*, mirroring 7–8 post-conception weeks (pcw) fetal lung bud tips (*19*). Collectively, these data strongly suggest that the d-LPC population in d-LO closely recapitulates the transcriptional profile and functional characteristics of early human lung bud tip cells.

Differentiation potential of d-LOs

While existing lung organoids model proximal airways or alveoli (*22*), respiratory bronchioles—a human-specific transitional zone—remain poorly modeled. To assess the fate potential of d-LOs in our system, we cultured p-LOs and d-LOs either in airway (DCIK) (*23*) or in alveolar (DCIK+CSB) media (*24*) (fig. S3A). We found that p-LO-derived airway organoids (p-AWO) expressed higher levels of proximal airway genes like *TP63* and *MUC5AC*, while d-LO-derived airway organoids (d-AWO) showed elevated expression of distal airway lineage genes, including *SCGB3A2* (a distal club cell marker), and alveolar lineage markers (*SFTPB*, *AGER*, *PDPN*, and *LAMP3*) (fig. S3B). For alveolar induction, only d-LOs cultured in DCIK+CSB media (d-ALO) exhibited robust alveolar differentiation, marked by high levels of *SFTPB*, *SFTPC*, *NKX2-1*, and *LAMP3*, consistent with the requirement of NKX2-1 for distal lung development. Notably, *SCGB3A2* was modestly expressed in d-ALO. Immunostaining further confirmed that d-LOs readily differentiate into distal airway and alveolar organoids, with abundant SCGB3A2 and SFTPB co-expressing cells, which are absent in p-AWO (fig. S3C). Collectively, these findings suggest that p-LOs

predominantly generate proximal airway organoids, while d-LOs uniquely model human distal airway and alveoli (fig. S3D).

Additionally, d-LO-derived organoids demonstrated functional properties, including CFTR-dependent forskolin swelling (fig. S4, A and B) and BODIPY-labeled phosphatidylcholine uptake and secretion (fig. S4, E and F). Beating cilia were visible (movie S1) in apical-out d-AWO released from Matrigel (*25*) (fig. S4C). Transmission electron microscopy (TEM) analysis of d-ALOs revealed lamellar body-like organelles (fig. S4D). In summary, these results indicate that d-LOs can efficiently generate distal airway and alveolar organoids with functional and structural features characteristic of mature lung tissue.

RAS cells in d-LO-derived organoids

To further investigate the unique cell type in d-LO-derived organoids, we performed scRNA-seq on p-AWO (D35), d-AWO (D35 and D90), and d-ALO (D35 and D90) (figs. S3A and S5, A and B). Cell populations were annotated using differentially expressed genes and correlated with established cell signatures from prior studies (*26*) (fig. S5, C and D). Both p-AWO and d-AWO showed abundant basal and proximal secretory cells, alongside smaller populations of club cells, ciliated cells, and pulmonary neuroendocrine cells (PNECs). AT2 cells were abundant in d-ALO (D90) (Fig. 2, A to C). Notably, we identified a distinct population of SCGB3A2^{+}SFTPB^{+}SFTPC^{-} cells, which we termed respiratory airway secretory cells (RAS cells), in d-LO-derived organoids, confirming their resemblance to human distal respiratory airways. This unique cluster was positioned between the d-LPC, proximal secretory, PNEC, and AT2 clusters on the UMAP embedding (Fig. 2A and fig. S5C), exhibited a specific gene expression profile, including markers such as *MUC1*, *CFTR*, *CEACAM6*, *SLC4A4*, and *STEAP4* (fig. S5E), with MUC1 and CEACAM6 serving as cell surface markers for these specialized secretory cells (*13, 27*).

Additionally, when transplanted under the kidney capsule of immunodeficient NSG mice, d-ALOs formed growths containing both tubular and saccular structures after 4 weeks (fig. S4, G to I). The tubular structures were lined by NKX2-1^{+}SCGB3A2^{+} epithelium, which also expressed SFTPB (Fig. 2D), mirroring the distal characteristics of human fetal lung tissue at 19 – 20-pcw (*14*). Collectively, these findings underscore the unique differentiation potential and functional relevance of d-LO-derived organoids in modeling human respiratory airways.

A d-LPC–RAS cell relationship

Research shows that SCGB3A2-expressing cells emerge as early as 5 pcw in fetal lungs (*28*). To explore the developmental trajectory of RAS cells, we integrated scRNA-seq data from d-LOs and d-LO-derived organoids (fig. S6, A to C). Trajectory inference analysis using Monocle3 revealed a strong cell trajectory originating from the d-LPC cluster into RAS cell cluster (Fig. 2, E to G). The gene expression changes along the d-LPC–RAS cell trajectory highlighted several genes known to be involved in secretory and alveolar differentiation, including *SCGB3A2*, *SFTPB* and *HOPX* (fig. S5, F and G). Additionally, transcription factors like *AHR*, *GRHL1*, and *SOX2*, identified through pseudotime analysis, showed strong correlations with primary distal airway secretory cells (*14*).

Further analysis of the integrated dataset demonstrated pseudotemporal relationships between RAS cells and basal, PNEC, and AT2 cells (Fig. 2, E and F, and fig. S6, D to G), indicating that RAS cells may function as progenitors for human distal lung development and regeneration. Trajectory inference also indicated a developmental link between p-LPC and ciliated cells (fig. S6H). Together, these in silico predictions suggest that d-LPC acts as a putative progenitor for the RAS cell lineage, which can subsequently give rise to basal, PNEC, and AT2 cells.

RAS cells exhibit immune functions

Transcriptomic profiling of the differentiation trajectory from d-LPC to RAS cell identified dynamic expression changes in genes associated with immune regulation, including *RUNX1*, *CD55*, *MUC1*, *SCGB3A2*, *TXNIP*, *CEBPD*, *S100A6*, and *S100A10*. Differential gene expression (DGE) analysis between d-LPCs and RAS cells further demonstrated elevated expression of immune-related transcripts in RAS cells, including mucins (*MUC1*, *MUC4*), surfactant proteins (*SFTPB*, *SFTPD*), cytokines (*CXCL8*, *CCL20*), and cell adhesion molecules (*ICAM5*, *ITGB6*) (Fig. 2H). Gene set enrichment analysis (GSEA) of the DEGs revealed significant enrichment of immune-associated pathways, such as antibacterial responses, regulation of viral entry into host cells, and positive regulation of pattern recognition receptor (PRR) signaling. These findings align with recent reports describing the immunomodulatory functions of TRB-SCs from the human distal airways (*14*). Together, these results establish a broad spectrum of immune-related transcriptional activity in RAS cells, emphasizing their pivotal role in respiratory immune defense.

RAS cells mount broad interferon-driven and inflammatory responses to RSV infection

Given the clinical relevance of RSV infection in distal airways in vulnerable individuals—particularly as a leading cause of bronchiolitis and pneumonia (*29*), we therefore evaluated RSV susceptibility using our distal organoid model (Fig. 3A).

RSV exhibited robust replication kinetics at a low multiplicity of infection (MOI = 0.1), as quantified in both supernatant and cell lysates (Fig. 3B). By 72 hpi, 62.7% of organoid cells were positive for RSV-F protein (Fig. 3D). Morphological analysis of infected d-ALOs revealed significant epithelial malformations, including cytoskeletal reorganization and syncytia formation (Fig. 3C), mirroring clinical hallmarks of RSV infection (*30*). Notably, SCGB3A2-positive cells were extensively targeted by RSV, as confirmed by co-staining of SCGB3A2 and RSV-F. Infected organoids exhibited substantial upregulation of inflammatory mediators (*CXCL8*, *CXCL10*, *TNF-a*, *IL-6*) (fig. S7A), contributing to immune cell recruitment and airway inflammation.

To further explore the cellular response, we performed scRNA-seq following RSV challenge. The scRNA-seq data revealed widespread infection, with viral transcripts detected in nearly all cells (Fig. 3E). However, viral gene expression was unevenly distributed, with most cells showing low viral transcript levels and two distinct clusters exhibiting significantly higher expression—one within RAS cells (RAS cell^{high}) and another among non-epithelial cells.

To characterize transcriptional changes specific to RAS cells upon infection, we conducted differential gene expression analysis between RAS cell^{high} and other infected clusters, as well as between RAS cell^{low} and mock-treated counterparts. Gene Ontology analysis of DEGs

revealed consistent enrichment of terms such as "response to virus" and "viral life cycle" across clusters (Fig. 3, F to I). Significant overlap was observed among DEGs from multiple comparisons, with strong enrichment for immune-related functions, including "defense response to virus", "antiviral innate immune response", "NF-kappa B signaling pathway", and "antigen presentation" (fig. S7, B and C). Furthermore, we observed elevated expression of PRRs, such as RIG-I (DDX58) and MDA5 (IFIH1), supporting robust viral RNA sensing and the downstream interferon pathway activation. Indeed, a broad range of interferon-stimulated genes (ISGs), including viral entry inhibitors (*MX1*, *MX2*, *IFITM1*, *TRIM22*), viral RNA degradation factors (*OAS1*, *OAS2*, *OAS3*, *OASL*), and the egress suppressor *RSAD2*, was induced, indicating a potent interferon-mediated antiviral state in RAS cells (Fig. 3K and fig. S7C). RAS cells also upregulated a panel of chemokines and inflammatory mediators, including *CXCL8*, *CXCL5*, *CCL20*, *CSF1*, and *TNFAIP3*, indicating their ability to recruit and modulate immune cell infiltration. Furthermore, elevated expression of *TAP1*, *CD274*, and *HLA-F* suggests partial engagement of antigen processing and adaptive immune signaling pathways. Strikingly, complement *C3* was consistently upregulated, supporting a previously underappreciated role for epithelial-derived complement in antiviral defense.

Together, these findings establish RAS cells as active immunological responders rather than passive targets during viral infection. They actively contribute to mucosal antiviral defense by orchestrating interferon responses, inflammatory signaling, and local complement activation.

RAS cells display antimicrobial responses via activation of TLR5

GSEA revealed significant enrichment of Toll-like receptor (TLR) signaling pathway genes in RAS cells (Fig. 2I), a pathway central to respiratory tract host defense (*31*). Notably, TLR5, a flagellin sensor, was specifically and highly expressed in RAS cells (fig. S7, D and E), which aligns with scRNA-seq data from early human fetal lung tissue identifying a SCGB3A2^{+}SFTPB^{+}CFTR^{+} subpopulation co-expressing TLR5 (*32*). Immunostaining further confirmed robust TLR5 protein expression in RAS cells within organoids (Fig. 4A).

To assess the functional role of TLR5 activation in RAS cells in response to flagellin, we treated our distal organoids with *Pseudomonas aeruginosa* (PAO1)-derived flagellin (FLA-PA) (Fig. 4B). Stimulation with FLA-PA significantly promoted the secretion of inflammatory mediators, including IL-6, CXCL8, CXCL10, and TNF-α (fig. S7F). This response was modestly attenuated by the TLR5-specific inhibitor TH1020 (Fig. 4C). To confirm RAS-specific responsiveness, AT2 cells were sorted using the HT2-280 antibody, and no immune response to FLA-PA was observed (fig. S7, G to I).

To further investigate the transcriptional response of RAS cells to TLR5 activation, we performed scRNA-seq on organoids treated with FLA-PA, with or without TH1020 (fig. S8, A to C). GSEA revealed significant induction of 29 canonical pathways in FLA-PA-treated RAS cells compared to controls (fig. S8, E to J and table S2). Among the top 15 enriched pathways, the majority were immune-related, including neutrophil chemotaxis/migration, antimicrobial peptide-mediated responses, Toll-like receptor signaling, and the humoral immune response (Fig. 4, D to F and fig. S8D). Under the GO term *humoral immune response*, 61 genes were significantly upregulated in RAS cells following FLA-PA exposure, encompassing chemokines, antimicrobial effectors, and epithelial-associated transcripts (Fig. 4G). Notably, multiple complement-related genes—including *C2*, *C3*, *CFB*, *CFHR1*,

CFHR5, *C4BPA*, *C8G*, and *CR2*—were markedly induced. The transcriptional activation of complement components is likely to facilitate opsonization and microbial clearance at the mucosal surface (*33*). Importantly, co-treatment with TH1020 substantially abolished the upregulation of these complement genes (Fig. 4G), while chemokine and antimicrobial gene expression persists to some extent. This suggests that the complement response is strictly TLR5-dependent, whereas the induction of chemokines and antimicrobial genes by FLA-PA may involve additional pathways, such as NOD2 signaling, in parallel with TLR5 activation. Furthermore, we observed a similar expression pattern in transplanted d-ALOs stimulated with flagellated bacteria PAO1 (Fig. 4, H to K).

These results reveal that RAS cells not only sense microbial threats via TLR5 but also mount a tiered defense response involving chemokine secretion, antimicrobial peptides, and complement activation. The unique TLR5 sensitivity of the complement module highlights a regulatory checkpoint linking epithelial sensing to immune effector coordination in distal airways.

COPD is associated with atypical immune activity of RAS cells

We next investigated whether similar or distinct immune programs are engaged by RAS cells in chronic disease settings, where infection and inflammation persist. To this end, we analyzed single-cell transcriptomic data from the terminal airway regions of COPD patients (*13*) (fig. S9, A to C). RAS cells from COPD lungs exhibited elevated expression of *TLR2*, *TLR3* and *TLR5* (Fig. 5A), accompanied by enhanced TLR signaling activity (fig. S9D), suggesting heightened epithelial pathogen sensing. Clinical evidence highlights the pathological relevance of PAO1 lung colonization in COPD (*34*). Immunostaining revealed increased co-expression of SFTPB, SCGB3A2, and TLR5 in infected COPD tissues compared to controls, along with robust expression of chemokines, implicating RAS cells in driving localized inflammation (fig. S9E).

Comparison of gene expression between healthy and COPD-derived RAS cells revealed differential enrichment of gene sets associated with extracellular matrix organization and mitochondrial ATP synthesis (fig. S9F and table S3), suggesting that RAS cells may participate in tissue remodeling, fibrosis, and metabolic adaptation through oxidative phosphorylation. Additionally, COPD RAS cells exhibited signatures of atypical immune activation and epithelial-intrinsic immune sensing (fig. S9, G to J).

Strikingly, GSEA revealed significant enrichment of the adaptive immune response in COPD RAS cells (Fig. 5B). A broad panel of antigen presentation–related genes and MHC components was upregulated (Fig. 5C), indicating that RAS cells may adopt noncanonical antigen-presenting cell (APC)-like properties. Concurrently, the increased expression of immunoglobulin-related transcripts (Fig. 5D) suggests that RAS cells may contribute to local antibody transport or expression, potentially amplifying immune responses to pathogens or facilitating immune complex deposition and chronic epithelial damage. Moreover, several immune regulatory genes, including *IRF1*, *RELB*, *SOCS5*, *RORA*, *TNFAIP3*, were elevated in COPD RAS cells (Fig. 5F), indicating a cytokine-instructed, interferon-responsive immune state. Notably, complement genes *C1R, C1S, C2*, and *C3* were markedly upregulated (Fig. 5E), with immunostaining confirming increased C3 protein expression (Fig. 5G). This persistent complement activity may exacerbate epithelial injury, amplify inflammation, and sustain pathogenic immune circuits. Together, these results demonstrate that RAS cells in

COPD adopt an immunologically active phenotype, potentially functioning as noncanonical antigen-presenting cells and contributors to chronic mucosal inflammation.

Discussion

The distal respiratory airways have long eluded functional investigation due to their anatomical inaccessibility and the inability of traditional rodent models to recapitulate their biology. By establishing a robust hPSC-derived distal lung organoid system, we overcome this challenge and identify RAS cells as key immunoregulatory sentinels of the human distal airways. Single-cell transcriptomic profiling mapped the differentiation trajectory of RAS cells from SOX9^{bright}NKX2-1^{bright} progenitors and revealed their multipotent capacity to generate basal cells, PNECs, and AT2 cells. Remarkably, our data reveal an unexpectedly broad spectrum of immune activity in RAS cells during both acute infection and chronic lung disease (Fig. 5h), spanning innate and adaptive axes, and suggest a potential epithelial–immune crosstalk mechanism driving chronic airway inflammation.

The evolutionary divergence between murine and human distal lung development significantly limits our understanding of specialized cellular niches, as the human distal lung exhibits greater branching complexity and an 8,000-fold larger surface area than its murine counterpart (*35, 36*). We show that RAS cells derive from SOX9^{bright}NKX2-1^{bright} bud tip progenitors and can differentiate into multiple lineages, establishing them as critical progenitors of the distal airway. Developmental lung disorders such as congenital pulmonary airway malformations (CPAM) (*37*) and bronchopulmonary dysplasia (BPD) (*38*), which involve abnormal small airway formation, may originate from disrupted differentiation trajectories of these progenitors. The plasticity of RAS cells likely evolved to enable repair and regeneration at the human distal respiratory airways (*39, 40*)— the initial site for gas exchange—underscoring their role in structural homeostasis.

Infections of the lower respiratory tract—ranging from respiratory bronchioles to alveoli—are leading causes of global morbidity and mortality (*41*). The unique cuboidal epithelium of the human distal airways, which lacks goblet cells and features sparse ciliation, requires alternative defense strategies distinct from proximal mucociliary clearance (*42*). We identify RAS cells as key immune sentinels of the distal airways. Our findings reveal that RAS cells execute essential immune surveillance, encompassing a range of immunological functions, including pathogen sensing, inflammatory signaling, antigen presentation, humoral coordination, and complement activation. RAS cells respond to diverse pathological contexts—including viral infection, bacterial exposure, and chronic inflammation (e.g., COPD)—by initiating robust and multifaceted immune programs that extend well beyond their traditional secretory roles.

Importantly, our study identifies complement component C3 as a converging effector induced in RAS cells under both acute and chronic inflammatory conditions. While previous studies have shown that C3 hyperactivation contributes to immunopathology in viral pneumonia, including COVID-19 (*43*), murine models have demonstrated that epithelial-derived C3 is also protective during bacterial pneumonia (*44*). Our study uncovers a regulatory mechanism of C3 expression through modulation of TLR5 signaling. The TLR5–complement pathway in RAS cells represents a promising therapeutic target. Modulating TLR5 signaling or downstream complement effector functions could provide novel strategies

to attenuate inflammation, preserve epithelial integrity, and restore immune balance in diseases such as viral bronchiolitis, bacterial pneumonia, and COPD.

Together, these findings establish RAS cells as dynamic, immunocompetent epithelial sentinels that actively monitor the airway microenvironment, coordinate front-line defenses, and interface with both innate and adaptive immunity to maintain distal airway homeostasis across health and disease. By elucidating the developmental origin, lineage plasticity, and immune functionality of RAS cells, we provide a conceptual framework for interpreting distal airway immunity and advancing epithelial-targeted therapies in respiratory disease. Future research should further define how dysregulated RAS cell immunity contributes to disease progression and how targeted intervention in these cells may offer therapeutic benefit.

References and Notes

1. R. J. Hewitt, C. M. Lloyd, Regulation of immune responses by the airway epithelial cell landscape. *Nat Rev Immunol* **21**, 347-362 (2021).
2. R. C. Mettelman, E. K. Allen, P. G. Thomas, Mucosal immune responses to infection and vaccination in the respiratory tract. *Immunity* **55**, 749-780 (2022).
3. E. R. Weibel, B. Sapoval, M. Filoche, Design of peripheral airways for efficient gas exchange. *Respir Physiol Neurobiol* **148**, 3-21 (2005).
4. E. R. Weibel, D. M. Gomez, Architecture of the human lung. Use of quantitative methods establishes fundamental relations between size and number of lung structures. *Science* **137**, 577-585 (1962).
5. P. R. Burgel *et al.*, Update on the roles of distal airways in COPD. *Eur Respir Rev* **20**, 7-22 (2011).
6. S. Booth *et al.*, A Single-Cell Atlas of Small Airway Disease in Chronic Obstructive Pulmonary Disease: A Cross-Sectional Study. *Am J Respir Crit Care Med* **208**, 472-486 (2023).
7. M. G. Pezet *et al.*, Human respiratory airway progenitors derived from pluripotent cells generate alveolar epithelial cells and model pulmonary fibrosis. *Nat Biotechnol*, (2025).
8. A. Vannan *et al.*, Spatial transcriptomics identifies molecular niche dysregulation associated with distal lung remodeling in pulmonary fibrosis. *Nat Genet*, (2025).
9. I. T. Stancil *et al.*, Pulmonary fibrosis distal airway epithelia are dynamically and structurally dysfunctional. *Nat Commun* **12**, 4566 (2021).
10. A. F. Rendeiro *et al.*, The spatial landscape of lung pathology during COVID-19 progression. *Nature* **593**, 564-569 (2021).
11. T. Flerlage, D. F. Boyd, V. Meliopoulos, P. G. Thomas, S. Schultz-Cherry, Influenza virus and SARS-CoV-2: pathogenesis and host responses in the respiratory tract. *Nat Rev Microbiol* **19**, 425-441 (2021).
12. L. Sikkema *et al.*, An integrated cell atlas of the lung in health and disease. *Nat Med* **29**, 1563-1577 (2023).

13. M. C. Basil *et al.*, Human distal airways contain a multipotent secretory cell that can regenerate alveoli. *Nature* **604**, 120-126 (2022).

14. P. Kadur Lakshminarasimha Murthy *et al.*, Human distal lung maps and lineage hierarchies reveal a bipotent progenitor. *Nature* **604**, 111-119 (2022).

15. S. Cao *et al.*, Single-cell RNA sequencing reveals the developmental program underlying proximal-distal patterning of the human lung at the embryonic stage. *Cell Res* **33**, 421-433 (2023).

16. E. E. Morrisey, B. L. Hogan, Preparing for the first breath: genetic and cellular mechanisms in lung development. *Dev Cell* **18**, 8-23 (2010).

17. P. Minoo, G. Su, H. Drum, P. Bringas, S. Kimura, Defects in tracheoesophageal and lung morphogenesis in Nkx2.1(-/-) mouse embryos. *Dev Biol* **209**, 60-71 (1999).

18. S. E. Kelly, C. J. Bachurski, M. S. Burhans, S. W. Glasser, Transcription of the lung-specific surfactant protein C gene is mediated by thyroid transcription factor 1. *J Biol Chem* **271**, 6881-6888 (1996).

19. K. Lim *et al.*, Organoid modeling of human fetal lung alveolar development reveals mechanisms of cell fate patterning and neonatal respiratory disease. *Cell Stem Cell* **30**, 20-37 e29 (2023).

20. A. J. Miller *et al.*, Generation of lung organoids from human pluripotent stem cells in vitro. *Nat Protoc* **14**, 518-540 (2019).

21. M. Crespo *et al.*, Colonic organoids derived from human induced pluripotent stem cells for modeling colorectal cancer and drug testing. *Nat Med* **23**, 878-884 (2017).

22. A. I. Vazquez-Armendariz, P. R. Tata, Recent advances in lung organoid development and applications in disease modeling. *J Clin Invest* **133**, (2023).

23. K. B. McCauley *et al.*, Efficient Derivation of Functional Human Airway Epithelium from Pluripotent Stem Cells via Temporal Regulation of Wnt Signaling. *Cell Stem Cell* **20**, 844-857 e846 (2017).

24. Y. Yamamoto *et al.*, Long-term expansion of alveolar stem cells derived from human iPS cells in organoids. *Nat Methods* **14**, 1097-1106 (2017).

25. J. Y. Co *et al.*, Controlling Epithelial Polarity: A Human Enteroid Model for Host-Pathogen Interactions. *Cell Rep* **26**, 2509-2520 e2504 (2019).

26. K. J. Travaglini *et al.*, A molecular cell atlas of the human lung from single-cell RNA sequencing. *Nature* **587**, 619-625 (2020).

27. A. S. Conchola *et al.*, Regionally distinct progenitor cells in the lower airway give rise to neuroendocrine and multiciliated cells in the developing human lung. *Proc Natl Acad Sci U S A* **120**, e2210113120 (2023).

28. A. Sountoulidis *et al.*, A topographic atlas defines developmental origins of cell heterogeneity in the human embryonic lung. *Nat Cell Biol* **25**, 351-365 (2023).

29. R. J. Pickles, J. P. DeVincenzo, Respiratory syncytial virus (RSV) and its propensity for causing bronchiolitis. *J Pathol* **235**, 266-276 (2015).

30. R. M. Liesman *et al.*, RSV-encoded NS2 promotes epithelial cell shedding and distal airway obstruction. *J Clin Invest* **124**, 2219-2233 (2014).

31. M. A. Kovach, T. J. Standiford, Toll like receptors in diseases of the lung. *Int Immunopharmacol* **11**, 1399-1406 (2011).

32. H. Quach *et al.*, Early human fetal lung atlas reveals the temporal dynamics of epithelial cell plasticity. *Nat Commun* **15**, 5898 (2024).

33. M. G. Detsika, K. Palamaris, I. Dimopoulou, A. Kotanidou, S. E. Orfanos, The complement cascade in lung injury and disease. *Respir Res* **25**, 20 (2024).

34. S. Qin *et al.*, Pseudomonas aeruginosa: pathogenesis, virulence factors, antibiotic resistance, interaction with host, technology advances and emerging therapeutics. *Signal Transduct Target Ther* **7**, 199 (2022).

35. H. Pan, G. H. Deutsch, S. E. Wert, S. Ontology, N. M. A. o. L. D. P. Consortium, Comprehensive anatomic ontologies for lung development: A comparison of alveolar formation and maturation within mouse and human lung. *J Biomed Semantics* **10**, 18 (2019).

36. M. C. Basil, E. E. Morrisey, Lung regeneration: a tale of mice and men. *Semin Cell Dev Biol* **100**, 88-100 (2020).

37. Y. Jiang *et al.*, Alteration of cystic airway mesenchyme in congenital pulmonary airway malformation. *Sci Rep* **9**, 5296 (2019).

38. A. Bhandari, S. McGrath-Morrow, Long-term pulmonary outcomes of patients with bronchopulmonary dysplasia. *Semin Perinatol* **37**, 132-137 (2013).

39. M. F. Beers, E. E. Morrisey, The three R's of lung health and disease: repair, remodeling, and regeneration. *J Clin Invest* **121**, 2065-2073 (2011).

40. B. L. Hogan *et al.*, Repair and regeneration of the respiratory system: complexity, plasticity, and mechanisms of lung stem cell function. *Cell Stem Cell* **15**, 123-138 (2014).

41. M. F. Lipscomb, J. Hutt, J. Lovchik, T. Wu, C. R. Lyons, The pathogenesis of acute pulmonary viral and bacterial infections: investigations in animal models. *Annu Rev Pathol* **5**, 223-252 (2010).

42. D. P. Hoytema van Konijnenburg, P. A. Nigrovic, I. Zanoni, Regional specialization within the mammalian respiratory immune system. *Trends Immunol* **45**, 871-891 (2024).

43. B. Yan *et al.*, SARS-CoV-2 drives JAK1/2-dependent local complement hyperactivation. *Sci Immunol* **6**, (2021).

44. S. K. Sahu *et al.*, Lung epithelial cell-derived C3 protects against pneumonia-induced lung injury. *Sci Immunol* **8**, eabp9547 (2023).

Acknowledgments: We thank the Imaging and Cell Technology Platforms, Guangzhou Laboratory for the confocal and flow cytometry. We acknowledge the use of ChatGPT for text editing to improve grammatical accuracy.

Funding: This work was supported by the

National Natural Science Foundation of China (82171419 to J.S.)

Major Project of Guangzhou National Laboratory (MP-GZNL2025C03007 to H.L.)

National Key Research and Development Program of China (2021YFA1101304 to H.L.)

National Key Research and Development Program of China (2020YFA0908200 to H.L.).

Author contributions:

Conceptualization: J.S., H.L.

Formal analysis: J.S., H.S., S.J.

Investigation: J.S., H.S., X.X.

Visualization: J.S., H.S., S.J.

Funding acquisition: H.L., J.S.

Project administration: J.S., H.L.

Resources: D.W., W.G., H.Y., H.Z., H.M.

Supervision: H.L., T.X., J.Z., W.K.Z.

Writing – original draft: J.S.

Writing – review & editing: H.L., W.K.Z., J.S.

Competing interests: Authors declare that they have no competing interests.

Data and materials availability: Organoids scRNA-seq data that support the findings of this study were deposited in the Gene Expression Omnibus under accession code GSE292679, and are publicly available. All data are available in the main text or the supplementary materials.

Supplementary Materials

Materials and Methods

Figs. S1 to S9

Tables S1 to S3

References (*45–49*)

Movies S1

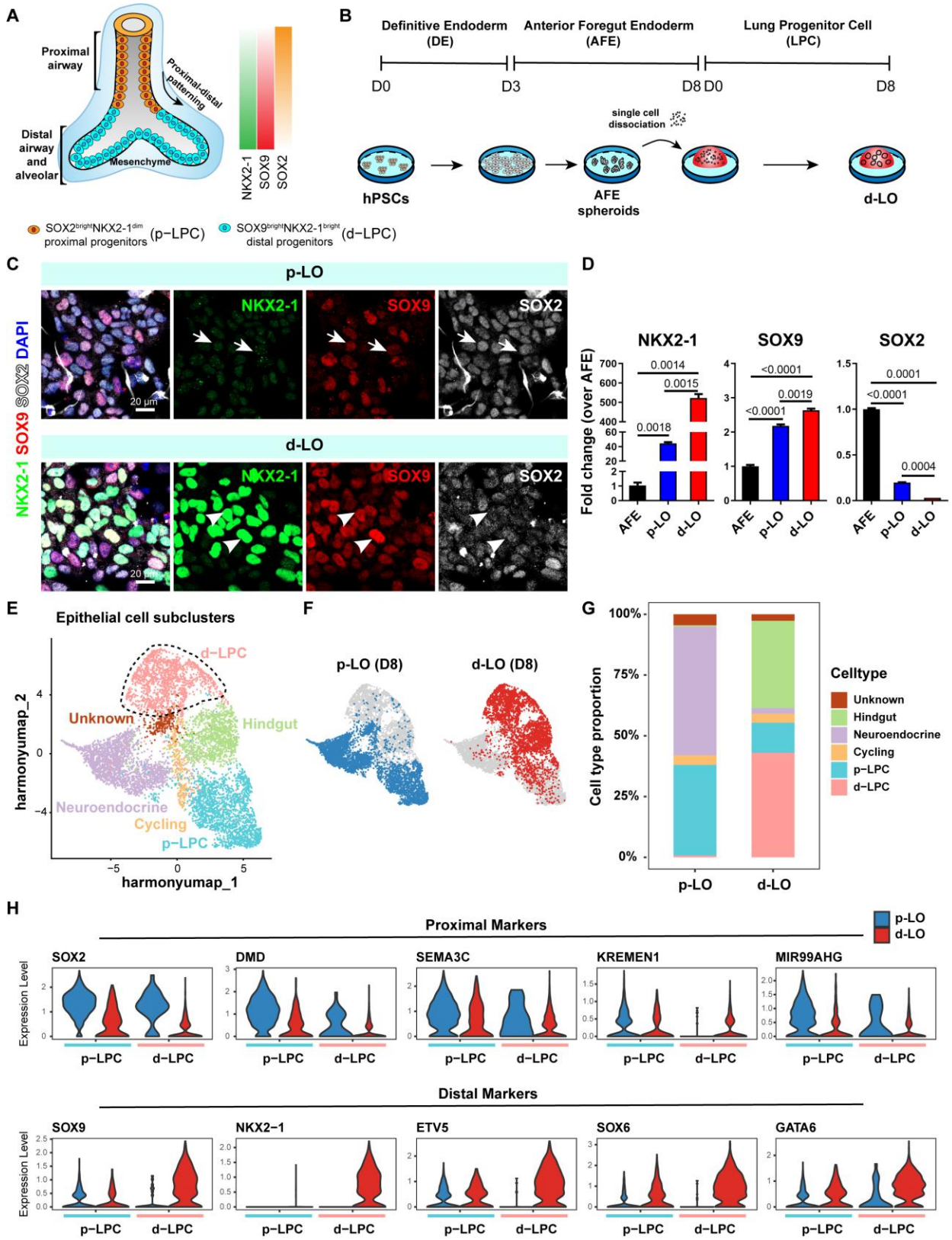
A
Proximal airway
Proximal-distal patterning
Distal airway and alveolar
Mesenchyme
NKX2-1
SOX9
SOX2
SOX2brightNKX2-1dim proximal progenitors (p−LPC)
SOX9brightNKX2-1bright distal progenitors (d−LPC)
B
Definitive Endoderm (DE)
Anterior Foregut Endoderm (AFE)
Lung Progenitor Cell (LPC)
D0
D3
D8 D0
D8
single cell dissociation
hPSCs
AFE spheroids
d-LO
C
p-LO
d-LO
NKX2-1 SOX9 SOX2 DAPI
20 µm
D
NKX2-1
SOX9
SOX2
Fold change (over AFE)
0.0014
0.0015
0.0018
<0.0001
0.0019
<0.0001
0.0001
<0.0001
0.0004
AFE
p-LO
d-LO
E
Epithelial cell subclusters
d−LPC
Unknown
Hindgut
Neuroendocrine
Cycling
p−LPC
harmonyumap_1
harmonyumap_2
F
p-LO (D8)
d-LO (D8)
G
Cell type proportion
100%
75%
50%
25%
0%
p-LO
d-LO
Celltype
Unknown
Hindgut
Neuroendocrine
Cycling
p−LPC
d−LPC
H
Proximal Markers
p-LO
d-LO
SOX2
DMD
SEMA3C
KREMEN1
MIR99AHG
Expression Level
p−LPC
d−LPC
Distal Markers
SOX9
NKX2−1
ETV5
SOX6
GATA6

Fig. 1. Robust induction of distal lung progenitor cells through AFE spheroid dissociation. (**A**) Schematic of proximal-distal patterning in developing human lung with representative lineage markers. (**B**) Differentiation protocol workflow from human pluripotent stem cells (hPSCs) to distal lung organoids (d-LOs) via dissociation of anterior foregut endoderm (AFE) spheroids. (**C**) Immunofluorescence staining of NKX2-1, SOX2 and SOX9 in proximal (p-LO) and distal (d-LO) lung organoids at day 8 LPC. White arrows denote SOX2^{bright}NKX2-1^{dim} cells; arrowheads indicate SOX9^{bright}NKX2-1^{bright} cells. Scale bars, 20 µm. Representative images from three biologically independent experiments. (**D**) Quantitative PCR analysis of *NKX2-1*, *SOX9* and *SOX2* expression in AFE spheroids, d-LOs, and p-LOs. Data are presented as mean ± SEM (n=3 biological replicates). *P*-values were calculated using an unpaired two-tailed Student's *t*-test with Welch's correction. (**E**) UMAP projection annotated with different epithelial cell subcluster identities. (**F**) Individual conditions of epithelial subclusters shown in (**E**). (**G**) Proportional distribution of cell types in d-LOs versus p-LOs. (**H**) Violin plots showing expression levels of proximal and distal markers in p-LPC and d-LPC cell populations derived from d-LOs and p-LOs.

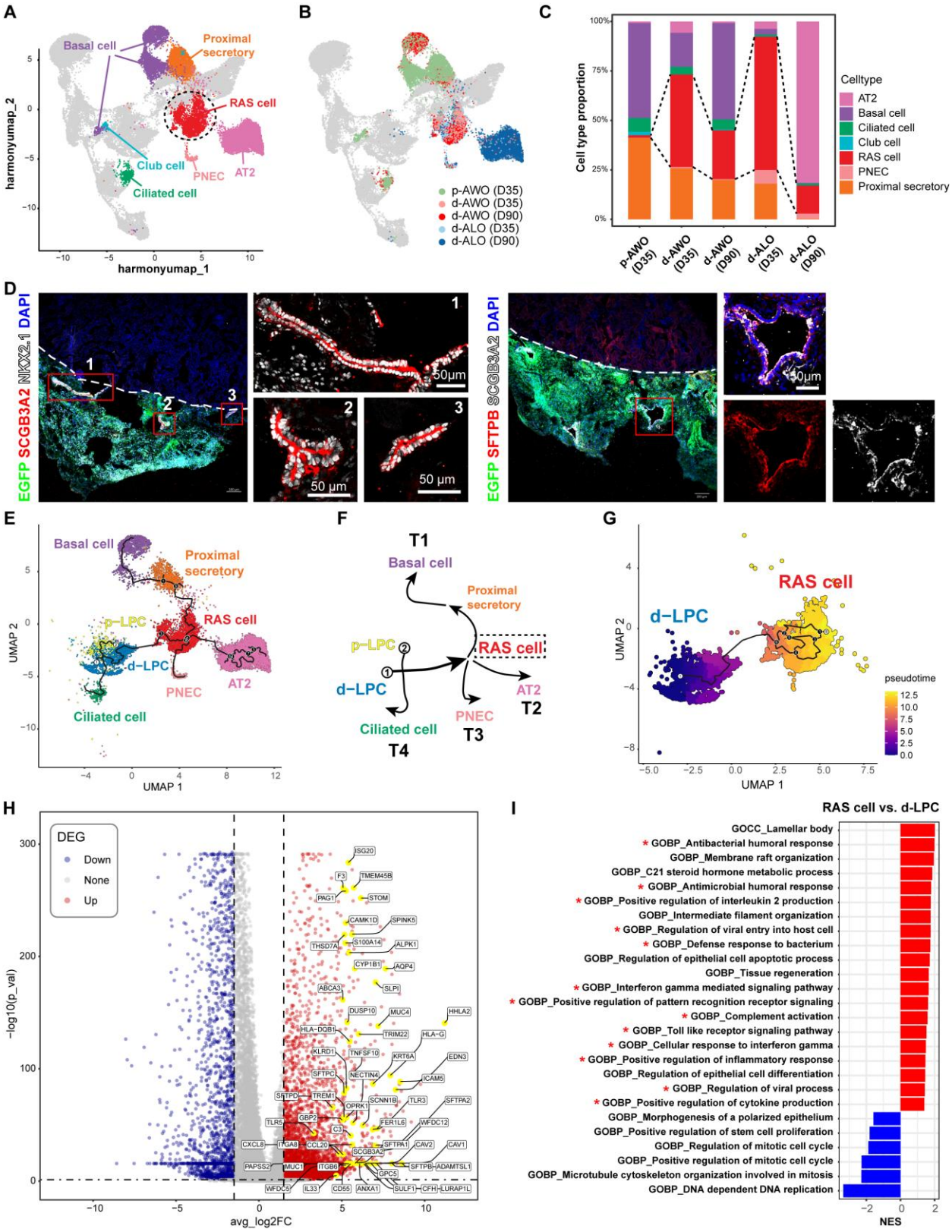
A
Basal cell
Proximal secretory
RAS cell
Club cell
PNEC
AT2
Ciliated cell
harmonyumap_2
harmonyumap_1
B
p-AWO (D35)
d-AWO (D35)
d-AWO (D90)
d-ALO (D35)
d-ALO (D90)
C
Cell type proportion
Celltype
AT2
Basal cell
Ciliated cell
Club cell
RAS cell
PNEC
Proximal secretory
p-AWO (D35)
d-AWO (D35)
d-AWO (D90)
d-ALO (D35)
d-ALO (D90)
D
EGFP SCGB3A2 NKX2.1 DAPI
EGFP SFTPB SCGB3A2 DAPI
50 μm
E
Basal cell
Proximal secretory
p-LPC
RAS cell
d-LPC
PNEC
AT2
Ciliated cell
UMAP 1
UMAP 2
F
T1
Basal cell
Proximal secretory
p-LPC
RAS cell
d-LPC
AT2
T2
PNEC
T3
Ciliated cell
T4
G
RAS cell
d-LPC
pseudotime
UMAP 1
UMAP 2
H
DEG
Down
None
Up
−log10(p_val)
avg_log2FC
I
RAS cell vs. d-LPC
GOCC_Lamellar body
GOBP_Antibacterial humoral response
GOBP_Membrane raft organization
GOBP_C21 steroid hormone metabolic process
GOBP_Antimicrobial humoral response
GOBP_Positive regulation of interleukin 2 production
GOBP_Intermediate filament organization
GOBP_Regulation of viral entry into host cell
GOBP_Defense response to bacterium
GOBP_Regulation of epithelial cell apoptotic process
GOBP_Tissue regeneration
GOBP_Interferon gamma mediated signaling pathway
GOBP_Positive regulation of pattern recognition receptor signaling
GOBP_Complement activation
GOBP_Toll like receptor signaling pathway
GOBP_Cellular response to interferon gamma
GOBP_Positive regulation of inflammatory response
GOBP_Regulation of epithelial cell differentiation
GOBP_Regulation of viral process
GOBP_Positive regulation of cytokine production
GOBP_Morphogenesis of a polarized epithelium
GOBP_Positive regulation of stem cell proliferation
GOBP_Regulation of mitotic cell cycle
GOBP_Positive regulation of mitotic cell cycle
GOBP_Microtubule cytoskeleton organization involved in mitosis
GOBP_DNA dependent DNA replication
NES

Fig. 2. Developmental trajectories and functional characterization of RAS cells. (**A**) UMAP embeddings colored by annotated cell types from single-cell RNA sequencing analysis of p-LO- and d-LO-derived organoids. (**B**) UMAP embeddings colored by differentiation time/media conditions. (**C**) Proportional distribution of lung lineage cell types in d-LO- and p-LO-derived organoids. (**D**) Immunofluorescence imaging of transplanted d-ALOs at 4 weeks post-engraftment. Triple staining for SCGB3A2 (red), EGFP (green), and NKX2-1 (grey) (left panel); SFTPB (red), EGFP (green), and SCGB3A2 (grey) (right panel). Scale bars, 100 μm (wide-field images), 50 μm (magnified images). Representative images from three biologically independent experiments. (**E**) Pseudotemporal trajectory reconstruction of epithelial subtypes using Monocle3. (**F**) Schematic summarizing developmental lineages inferred from pseudotemporal analysis in (**E**). (**G**) Differentiation trajectory connecting d-LPCs to RAS cells. (**H**) Volcano plot of differentially expressed genes (DEGs) between d-LPCs and RAS cells. (**I**) Gene set enrichment analysis (GSEA) of DEGs from (**H**), ranked by normalized enrichment score (NES).

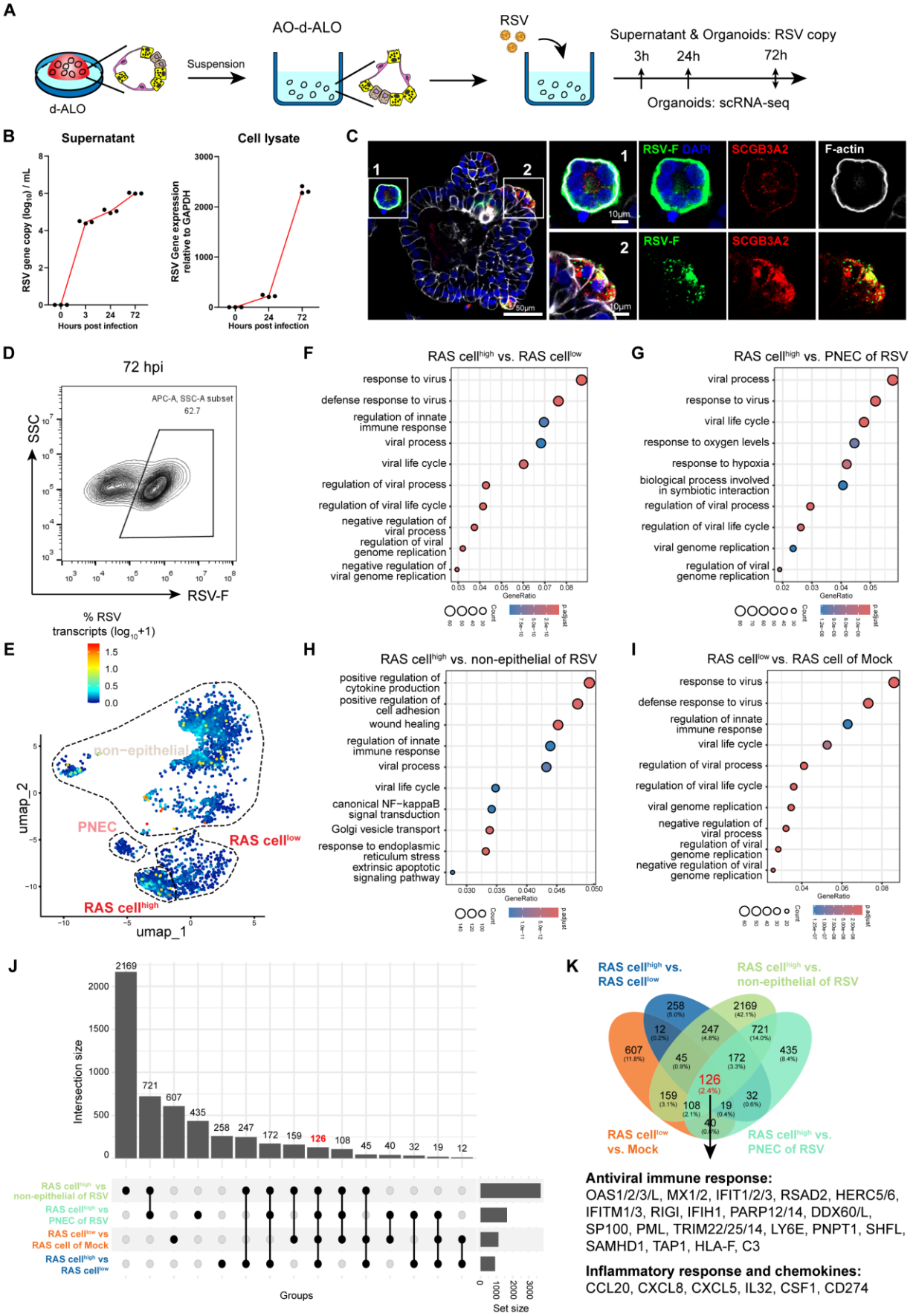
A
d-ALO
Suspension
AO-d-ALO
RSV
Supernatant & Organoids: RSV copy
3h
24h
72h
Organoids: scRNA-seq
B
Supernatant
Cell lysate
RSV gene copy (log10) / mL
RSV Gene expression relative to GAPDH
Hours post infection
C
RSV-F DAPI
SCGB3A2
F-actin
RSV-F
SCGB3A2
10μm
50μm
D
72 hpi
APC-A, SSC-A subset
62.7
SSC
RSV-F
E
% RSV transcripts (log10+1)
non-epithelial
PNEC
RAS cellhigh
RAS cellhigh
umap_1
umap_2
F
RAS cellhigh vs. RAS cellhigh
response to virus
defense response to virus
regulation of innate immune response
viral process
viral life cycle
regulation of viral process
regulation of viral life cycle
negative regulation of viral process
regulation of viral genome replication
negative regulation of viral genome replication
GeneRatio
G
RAS cellhigh vs. PNEC of RSV
viral process
response to virus
viral life cycle
response to oxygen levels
response to hypoxia
biological process involved in symbiotic interaction
regulation of viral process
regulation of viral life cycle
viral genome replication
regulation of viral genome replication
GeneRatio
H
RAS cellhigh vs. non-epithelial of RSV
positive regulation of cytokine production
positive regulation of cell adhesion
wound healing
regulation of innate immune response
viral process
viral life cycle
canonical NF-kappaB signal transduction
Golgi vesicle transport
response to endoplasmic reticulum stress
extrinsic apoptotic signaling pathway
GeneRatio
I
RAS cellhigh vs. RAS cell of Mock
response to virus
defense response to virus
regulation of innate immune response
viral life cycle
regulation of viral process
regulation of viral life cycle
viral genome replication
negative regulation of viral process
regulation of viral genome replication
negative regulation of viral genome replication
GeneRatio
J
Intersection size
2169
721
607
435
258
247
172
159
126
108
45
40
32
19
12
RAS cellhigh vs non-epithelial of RSV
RAS cellhigh vs PNEC of RSV
RAS cellhigh vs RAS cell of Mock
RAS cellhigh vs RAS cellhigh
Groups
Set size
K
RAS cellhigh vs. RAS cellhigh
RAS cellhigh vs. non-epithelial of RSV
RAS cellhigh vs. PNEC of RSV
RAS cellhigh vs. RAS cell of Mock
258 (5.0%)
2169 (42.1%)
12 (0.2%)
247 (4.8%)
721 (14.0%)
607 (11.8%)
435 (8.4%)
45 (0.9%)
172 (3.3%)
126 (2.4%)
159 (3.1%)
108 (2.1%)
19 (0.4%)
32 (0.6%)
40 (0.8%)
Antiviral immune response:
OAS1/2/3/L, MX1/2, IFIT1/2/3, RSAD2, HERC5/6, IFITM1/3, RIGI, IFIH1, PARP12/14, DDX60/L, SP100, PML, TRIM22/25/14, LY6E, PNPT1, SHFL, SAMHD1, TAP1, HLA-F, C3
Inflammatory response and chemokines:
CCL20, CXCL8, CXCL5, IL32, CSF1, CD274

Fig. 3. Enhanced antiviral activity of RAS cells during RSV infection. (**A**) Schematic illustration of the procedure for RSV infection in d-ALOs. (**B**) RSV replication kinetics in d-ALOs quantified by RT – qPCR of viral RNA in supernatants (left) and cell lysates (right) at indicated time points. Each dot represents one well (n = 3 biological replicates). (**C**) Morphological changes in d-ALOs post-RSV infection. Left: overview; right: magnified regions showing cytopathic effects. Scale bars, 50 µm (overview), 10 µm (magnified images). Representative images from three independent experiments. (**D**) Infection efficiency in d-ALOs assessed by flow cytometry analysis of RSV-F glycoprotein expression at 72 hpi (MOI= 0.1). (**E**) UMAP projection of single-cell transcriptomes colored by the percentage of viral transcripts per cell. (**F** to **I**) Gene Ontology (GO) enrichment analysis of differentially expressed genes (DEGs) identified in the following comparisons: (**F** to **G**) RAS cell^{high} versus Other clusters in infected organoids and (**I**) RAS cell^{low} versus Mock. (**J** to **K**) Venn diagrams illustrating shared DEGs between RAS cell^{high} versus Other clusters (Infected), and RAS cell^{low} versus the same cluster in mock.

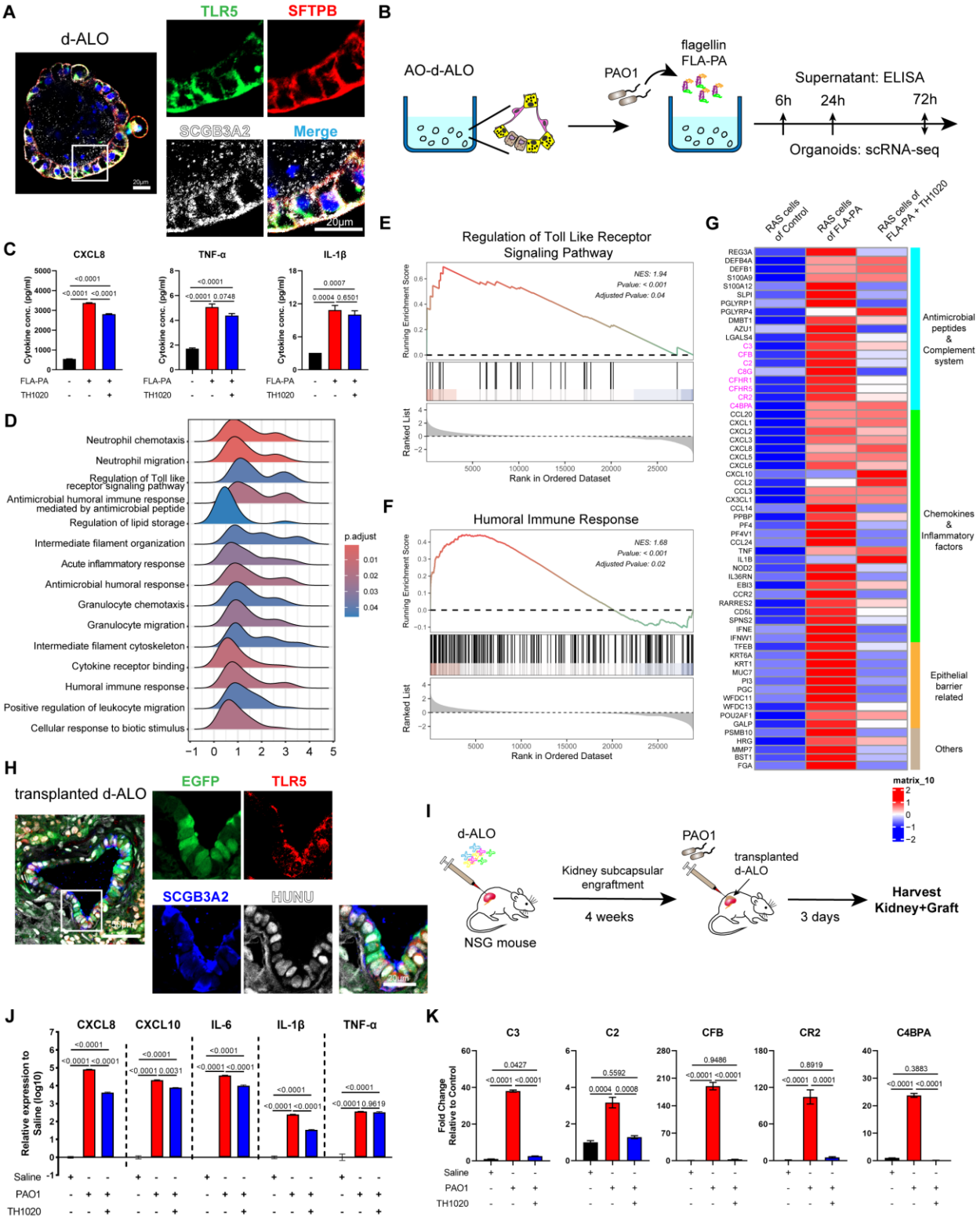
A
d-ALO
TLR5
SFTPB
SCGB3A2
Merge
20μm
B
AO-d-ALO
PAO1
flagellin
FLA-PA
Supernatant: ELISA
6h
24h
72h
Organoids: scRNA-seq
C
CXCL8
TNF-α
IL-1β
Cytokine conc. (pg/ml)
FLA-PA
TH1020
D
Neutrophil chemotaxis
Neutrophil migration
Regulation of Toll like receptor signaling pathway
Antimicrobial humoral immune response mediated by antimicrobial peptide
Regulation of lipid storage
Intermediate filament organization
Acute inflammatory response
Antimicrobial humoral response
Granulocyte chemotaxis
Granulocyte migration
Intermediate filament cytoskeleton
Cytokine receptor binding
Humoral immune response
Positive regulation of leukocyte migration
Cellular response to biotic stimulus
p.adjust
E
Regulation of Toll Like Receptor Signaling Pathway
NES: 1.94
Pvalue: < 0.001
Adjusted Pvalue: 0.04
Running Enrichment Score
Ranked List
Rank in Ordered Dataset
F
Humoral Immune Response
NES: 1.68
Pvalue: < 0.001
Adjusted Pvalue: 0.02
G
RAS cells of Control
RAS cells of FLA-PA
RAS cells of FLA-PA + TH1020
Antimicrobial peptides & Complement system
Chemokines & Inflammatory factors
Epithelial barrier related
Others
matrix_10
H
transplanted d-ALO
EGFP
TLR5
SCGB3A2
HUNU
20μm
I
d-ALO
NSG mouse
Kidney subcapsular engraftment
4 weeks
PAO1
transplanted d-ALO
3 days
Harvest Kidney+Graft
J
CXCL8
CXCL10
IL-6
IL-1β
TNF-α
Relative expression to Saline (log10)
Saline
PAO1
TH1020
K
C3
C2
CFB
CR2
C4BPA
Fold Change Relative to Control

5

Fig. 4. TLR5 activation mediates microbial-induced immune responses in RAS cells. (**A**) Whole-mount immunofluorescence staining for TLR5 (green) and RAS cell markers (SFTPB, red and SCGB3A2, grey) in d-ALO. Nuclei counterstained with Hoechst (blue). Scale bars, 20 μm. Representative of three independent experiments. (**B**) Schematic illustration of the procedure for FLA-PA treatment in d-ALOs. (**C**) Secretion of cytokines/chemokines (CXCL8, CXCL10, IL-6, IL-1β, TNF-α) from d-ALOs stimulated with 1 μg/ml FLA-PA protein for 72 hours, with or without 1 μM TLR5 inhibitor TH1020. (**D**) Top 15 GO terms enriched in DEGs between FLA-PA-treated RAS cells and control RAS cells. (**E**, **F**) Gene Set Enrichment Analysis (GSEA) plots showing up-regulation of the TLR signaling pathway (**E**) and the humoral immune response (**F**) in FLA-PA-treated RAS cells compared to control RAS cells. (**G**) Expression profiles of genes enriched in the "humoral immune response" pathway (from GSEA) across control, FLA-PA-treated, and FLA-PA+TH1020-treated RAS cells. (**H**) Immunofluorescence co-staining for TLR5 (red), SCGB3A2 (blue), and human nuclear antigen (HUNU, white) in transplanted d-ALOs at 4 weeks post-engraftment in NSG mice. Scale bars, 50 μm (low-magnification images), 20 μm (magnified images). Representative of three independent transplants. (**I**) Schematic illustration of the procedure for PAO1 infection in transplanted d-ALOs. (**J**) Quantitative PCR analysis of inflammatory mediators in transplanted d-ALOs stimulated with PAO1 lysate for 72 hours, with or without 1 μM TH1020 treatment. (**K**) Quantitative PCR analysis of complement-related genes in PAO1 lysate-stimulated transplanted d-ALOs with or without 1 μM TH1020 (72 h). (**C**,**J**,**K**) Data are presented as mean values ± SEM. *P*-values were calculated by one-way ANOVA with Tukey's multiple comparison test (n=3 biological replicates).

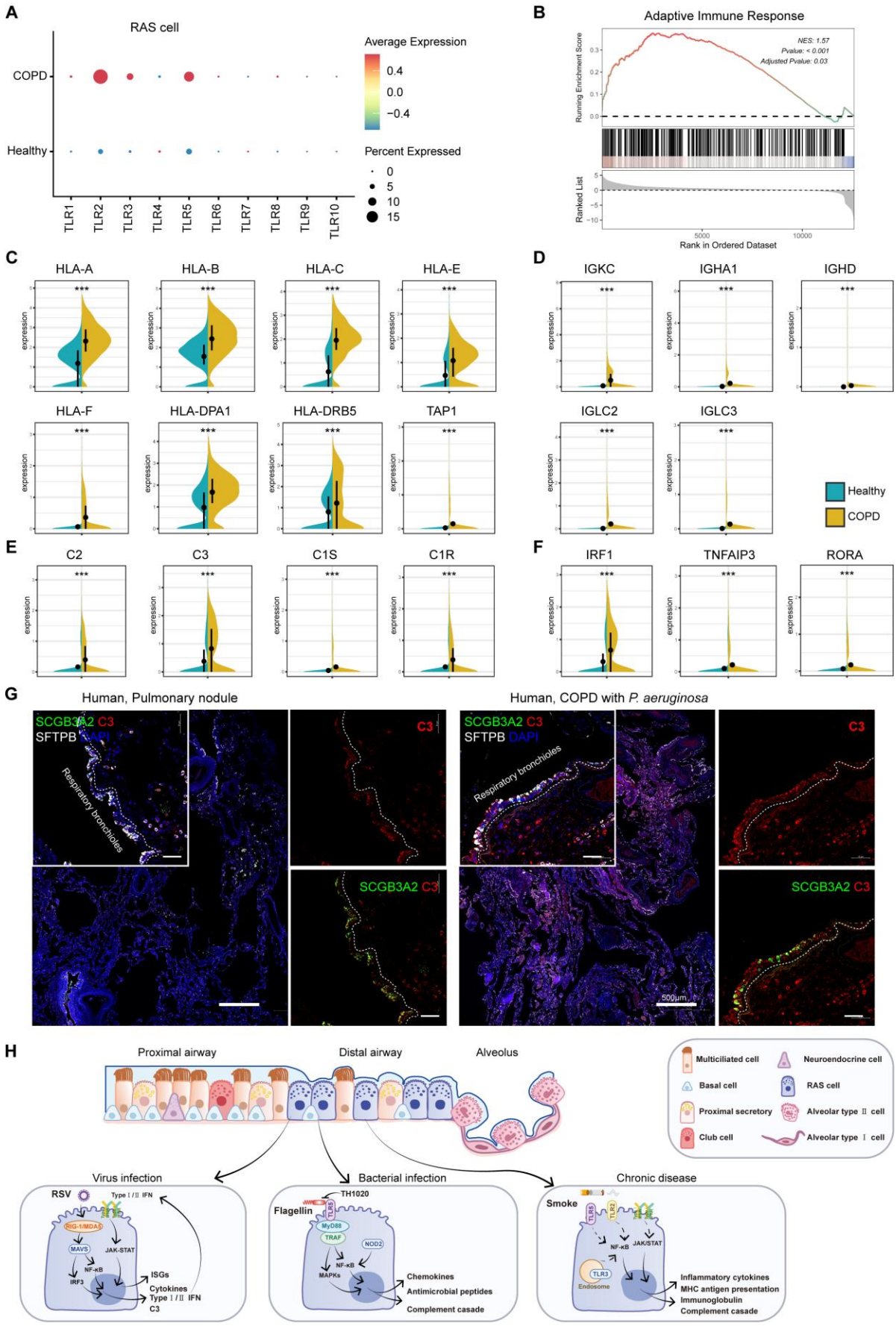
A
RAS cell
COPD
Healthy
TLR1
TLR2
TLR3
TLR4
TLR5
TLR6
TLR7
TLR8
TLR9
TLR10
Average Expression
0.4
0.0
−0.4
Percent Expressed
0
5
10
15
B
Adaptive Immune Response
NES: 1.57
Pvalue: < 0.001
Adjusted Pvalue: 0.03
Running Enrichment Score
Ranked List
Rank in Ordered Dataset
C
HLA-A
HLA-B
HLA-C
HLA-E
HLA-F
HLA-DPA1
HLA-DRB5
TAP1
D
IGKC
IGHA1
IGHD
IGLC2
IGLC3
Healthy
COPD
E
C2
C3
C1S
C1R
F
IRF1
TNFAIP3
RORA
G
Human, Pulmonary nodule
Human, COPD with P. aeruginosa
SCGB3A2 C3
SFTPB DAPI
Respiratory bronchioles
C3
500μm
H
Proximal airway
Distal airway
Alveolus
Multiciliated cell
Neuroendocrine cell
Basal cell
RAS cell
Proximal secretory
Alveolar type Ⅱ cell
Club cell
Alveolar type Ⅰ cell
Virus infection
RSV
Type Ⅰ/Ⅲ IFN
RIG-I/MDA5
MAVS
JAK-STAT
NF-κB
IRF3
ISGs
Cytokines
Type Ⅰ/Ⅲ IFN
C3
Bacterial infection
TH1020
Flagellin
TLR5
MyD88
TRAF
NOD2
NF-κB
MAPKs
Chemokines
Antimicrobial peptides
Complement casade
Chronic disease
Smoke
TLR8
TLR2
NF-κB
JAK/STAT
TLR3
Endosome
Inflammatory cytokines
MHC antigen presentation
Immunoglobulin
Complement casade

Fig. 5. COPD is associated with enhanced immune activity in RAS cells. (**A**) Expression of Toll-like receptors (TLRs) in RAS cell clusters from COPD and healthy controls. (**B**) GSEA plot showing up-regulation of the adaptive immune response pathway in RAS cell clusters from COPD patients compared to those from healthy controls. (**C** to **F**) Violin plots illustrating expression levels of selected genes contributing to the Gene Ontology (GO) biological process 'adaptive immune response'. (**G**) Confocal immunofluorescence images of SCGB3A2 (green), C3 (red), SFTPB (white), and DAPI (blue) in human lung sections from control individuals and *Pseudomonas aeruginosa*-infected COPD patients. White boxed areas are expanded. Scale bars, 50 μm. Representative of two patients per condition. (**H**) Schematic diagram summarizing the immunity role of RAS cells in acute infections (viral and bacterial) and chronic inflammatory disease (COPD).